Photoresponsive Materials

DOI: 10.1002/ange.201306763

Enhancement of the Photoresponse in Organic Field-Effect Transistors by Incorporating Thin DNA Layers**

*Yuan Zhang, Mingfeng Wang, Samuel D. Collins, Huiqiong Zhou, Hung Phan, Christopher Proctor, Alexander Mikhailovsky, Fred Wudl, and Thuc-Quyen Nguyen**

Abstract: *A mechanistic study of the DNA interfacial layer that enhances the photoresponse in n-type field-effect transistors (FET) and lateral photoconductors using a solution-processed fullerene derivative embedded with disperse-red dye, namely PCBDR, is reported. Incorporation of the thin DNA layer simultaneously leads to increasing the electron injection from non-Ohmic contacts into the PCBDR active layer in dark and to increasing the photocurrent under irradiation. Such features lead to the observation of the enhancement of the photoresponsivity in PCBDR FETs up to 10^3. Kelvin probe microscopy displays that in the presence of the DNA layer, the surface potential of PCBDR has a greater change in response to irradiation, which is rationalized by a larger number of photoinduced surface carriers. Transient absorption spectroscopy confirms that the increase in photoinduced carriers in PCBDR under irradiation is primarily ascribed to the increase in exciton dissociation rates through the PCBDR/DNA interface and this process can be assisted by the interfacial dipole interaction.*

Organic field-effect transistors (OFET) offer vast promises in large-area displays, sensor arrays, and flexible electronics with low-cost fabrication.[1–6] An attractive property of OFETs is afforded by the tunable photoresistivity, allowing applications in light-sensitive optoelectronics including photodetectors, light-induced switches, light-triggered amplifiers, and image sensors.[7–14] In comparison to conventional OFETs that are operated in dark, organic phototransistors (OPT) require both satisfactory charge transport and high photoresponse to render the detection mechanism.[15–17] When using bulk heterojunction (BHJ) structure, one seeks an organic electron donor/acceptor blend system to increase the photon-to-charge conversion rate and resultant light sensitivity.[12,18] This concept has been successfully applied to organic photodiodes with a sandwich device geometry.[10,19,20] However, for OPTs containing electron donor/acceptor active layers, ambipolar behaviors are often observed. As a result, the off-state current of OPTs can be lifted, which reduces the detectivity.[21,22] OPTs based on single active components have been shown with the capability of delivering the dual-functionality of photo- and electronic switches.[23–26] The light sensitivity of OPTs are found heavily affected by bulk material properties including molecular structure,[27,28] morphology, and crystallinity of the photoactive material[29] and also the device dimension.[30] In these OPTs, the active layer generally consists of a p-type semiconductor whereas OPTs using n-type semiconductors are sparingly reported. An exclusive example refers to the active materials of perylene derivatives, which have a strong electron affinity, high stability[31,32] and large photoresponsivity (up to 4.1×10^5 AW^{-1}) when used for solution-processed OPTs.[30]

In addition to bulk properties, interfacial effects are crucial in dictating the OPT operation. In principle, one needs to deal with the organic/electrode interface where charges are efficiently extracted towards the electrodes under irradiation while the dark current is suppressed to achieve a high photoresponse. Interlayers comprising DNA thin films have been previously demonstrated with the ability of mediating charge injection in organic light-emitting diodes (OLED) and ambipolar OFETs.[33,34] The reduced electron injection barrier by thin DNA layers is attributable to the interfacial dipole interaction, allowing to modify the work functions (WF) of metal electrodes. These features led to an increase in the luminance efficiencies (in PLEDs) and field-effect mobilities (in ambipolar OFETs) when incorporating the DNA layer.[34–36]

Here, we investigate the effects of thin DNA layers on the photoresponse of solution-processed n-type OPTs and lateral diodes. The active layer is based on a new fullerene chromophore 1-(3-carboxypropyl)-1-phenyl[6,6]C61 (PCBA) incorporated with a disperse-red dyad, denoted as PCBDR that features an absorption in the range of 400–600 nm.[37] By incorporating the DNA layer, a considerable increase in the photocurrent is observed leading to a photosensitivity (P) exceeding 10^3 upon irradiation. The increased photocurrent is rationalized by the combined results of the modified electron

[*] Dr. Y. Zhang, S. D. Collins, Dr. H. Zhou, H. Phan, C. Proctor, Dr. A. Mikhailovsky, Prof. F. Wudl, Prof. T.-Q. Nguyen
Center for Polymers and Organic Solids
University of California, Santa Barbara
Santa Barbara, CA 93106 (USA)
E-mail: quyen@chem.ucsb.edu
Prof. M. Wang
Division of Chemical and Biomolecular Engineering
School of Chemical and Biochemical Engineering
Nanyang Technologycal Univeristy
62 Nanyang Drive, 637459, Singapore (Singapore)

[**] Financial support for this work is from the Department of Energy Office of Basic Energy Sciences (grant number DE-SC0002368). T.Q.N. thanks the Camille Dreyfus Teacher Scholar Award and the Alfred Sloan Research Fellowship program. M.W. thanks the Natural Sciences and Engineering Research Council of Canada for a Post-doctoral Fellowship (grant number PDF-373502-2009). We thank the group of David Ginger at University of Washington for providing us a copy of their SKPM code. We are also grateful to R. Naik, F. Ouchen, and J. G. Grote (AFRL) for providing the DNA material.

Supporting information for this article is available on the WWW under http://dx.doi.org/10.1002/anie.201306763.

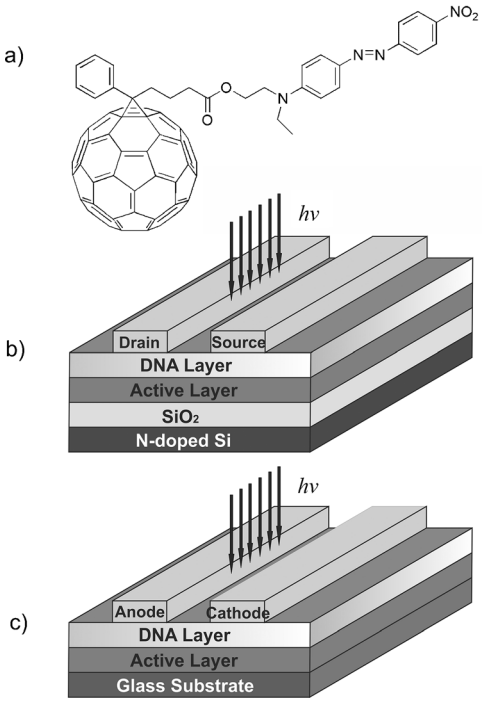

Figure 1. a) Chemical structure of PCBDR. Device structures of b) PCBDR transistors and c) planar diodes incorporating the thin DNA layer. Black arrows: Illustration of the incident white light perpendicular to the active layer sourced by a xenon lamp with AM 1.5 G filter.

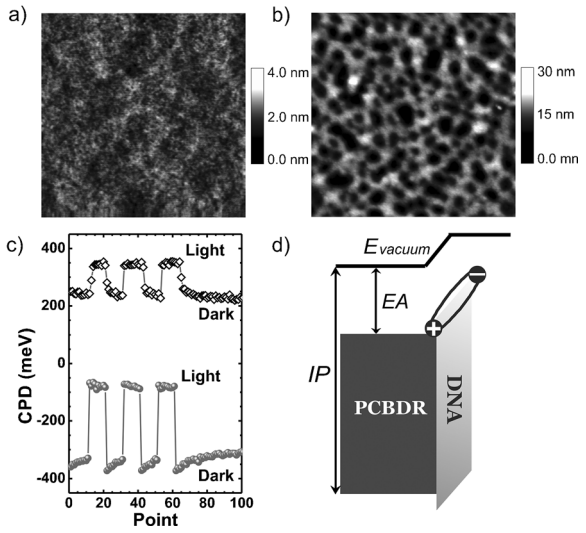

Figure 2. AFM topographic images (2 μm × 2 μm) of a) PCBDR and b) PCBDR/DNA films. c) Switch of the surface CPD of PCBDR (black open diamonds) and PCBDR/DNA (gray filled circles) films with the switching of the irradiation between dark and about 100 mW cm^{-2}. d) Energy diagram of the PCBDR with the DNA layer. The oval denotes the orientation of the interfacial dipole.

injection and enhanced exciton dissociation at the PCBDR/metal interface.

The chemical structure of PCBDR is provided in Figure 1 a. The structural similarity of PCBDR with [6,6]-phenyl-C61-butyric acid methyl ester ($PC_{61}BM$) leads to n-type transport behavior while the absorption at 480 nm by the disperse-red moiety in PCBDR facilitates the sensitization in the visible range.[37] Figure 1 b illustrates the device structure of n-type OPTs using a staggered geometry. For the lateral diode, the same device configuration is used except for the glass substrates. For the OPT or lateral diode, PCBDR-active layers were spin cast atop the Si/SiO_2 or glass substrates, leading to a film thickness of around 60 nm. The DNA was deposited from the methanol:H_2O solvent mixture (9:1 vol) on top of the PCBDR-active layer and the optimal film thickness was approximately 10 nm as confirmed by atomic force microscopy (AFM). Details of preparation of the DNA solution and films deposition are described elsewhere.[33] Finally, 80 nm Al or Au source–drain electrodes were thermally evaporated through shadow masks. The black arrows sketched in Figure 1 illustrate the incident continuous wavelength (cw) white light using a xenon lamp with AM 1.5 G filter. The light was perpendicularly shined onto the OPT conduction channel.

Figure 2 a and b shows 2 μm × 2 μm AFM height images for PCBDR films without and with the deposition of the DNA layer. The film of PCBDR, similar to PCBM shows an amorphous, featureless and smooth surface with an average roughness of 0.3 nm.[34] After depositing the DNA layer, we observe a changed surface morphology showing network-like structures. This is similar to the features observed on DNA surfaces when deposited on top of poly[2-methoxy-5-(2-ethylhexyloxy)-1,4-phenylenevinylene] (MEH-PPV).[33] The surface roughness of PCBDR/DNA films drastically increases to 3 nm. The different surface morphology of the PCBDR/DNA film indicates the coverage of DNA on PCBDR. Figure S1 (in the Supporting Information) shows electrostatic force microscopy (EFM) 1ω images of PCBDR and PCBDR/DNA films prepared on ITO substrates.[38–40] When applying a bias of −0.28 V that cancels out the contact potential difference (CPD) between the conducting Pt/Ir tip and conducting ITO substrate, the surface charge polarity is representatively described by the average of the differential frequency shift ($\Delta\omega$) in the 1ω EFM image.[40] We observe an average $\Delta\omega$ of −36.4 Hz and 19.7 Hz for PCBDR films with and without the DNA, respectively. Based on the model proposed by Brus and co-workers, the result suggests that the PCBDR/DNA surface possesses positive electrostatic charges.[40]

Figure 2 c compares switches of the surface contact potential difference (CPD) of PCBDR and PCBDR/DNA films along with the switching of irradiation (between dark and about 100 mW cm^{-2} cw light) measured by Kelvin probe force spectroscopy. In dark, the CPD of the PCBDR/DNA exhibits a 530 mV shift, which is ascribed to the change in the surface electronic potential induced by DNA. Under irradiation, we observe a deepening of the surface CPD (here a more positive CPD means a deeper electrical potential with regard to the vacuum level), which is due to light-induced carriers. To enable a meaningful comparison, we define the difference between the CPD in dark and under irradiation (Δ_{CPD}) as $\Delta_{CPD} = CPD_{(light)} - CPD_{(dark)}$. In the presence of the DNA layer, we observe an increase in Δ_{CPD} from 107 to

270 meV and the Δ_{CPD} is reversible with the switch of irradiation. The enlargement of Δ_{CPD} may indicate a larger surface charge carrier density changes upon irradiation in the presence of DNA layers.

Figure S2 shows the X-ray photoemission spectroscopy (XPS) of PCBDR and PCBDR/DNA films. The XPS spectra of PCBDR/DNA show two unique peaks at 133.1 and 1070.6 eV that are assigned to phosphorus (P) 2p and sodium (Na) 1s photoelectrons, respectively. In contrast, we do not observe these two peaks in the pristine PDBDR. Appearance of the distinctive XPS of PCBDR/DNA can be correlated with the present phosphate function groups in DNA, which has been previously rationalized for the creation of an interfacial dipole at the $PC_{70}BM$/DNA interface.[34] In combination of these features, we propose an energy diagram of PCBDR in contact with a metal electrode as shown in Figure 2d. At the DNA/PCBDR interface, the interfacial dipole leads to a noticeable band bending. The orientation of the dipole depicted by the oval in Figure 2c is likely to result in an upward shift of the vacuum level at the PCBDR/DNA interface.

Next we examine the impact of the DNA layer on the photoresponse of PCBDR OPTs. Figure 3a and b compare dark and irradiated (irradiation intensity $P_{light} = 2.9\ mW\,cm^{-2}$) output characteristics ($V_g = +60$ V) of the PCBDR OPTs with (left panels) and without (right panels) incorporating the DNA layer using Al source–drain electrodes. At first we examine the change in device characteristics in dark with the DNA layer. As can be seen, the current (I_{ds}) of the PCBDR/DNA OPT substantially increases, for example, from 0.021 to 0.14 μA with $V_d = +60$ V (also see Figure S4a in the Supporting Information for results using Au source–drain electrodes). The threshold voltage (V_{th}) and turn-on voltage (V_{on}) also dramatically reduce as shown in Figure S4c. The enhancement of I_{ds} is explained by the reduced electron injection barrier Φ_e,[34] defined as $\Phi_e = LUMO - WF$. Similarly, we observe an enhanced I_{ds} in the presence of the DNA layer for OPTs using Au electrodes (Figure S4a and S4b). To confirm the effect of improved electron injection by DNA, we measured the WF of Al and Au electrodes without and with deposition of DNA on top. As shown by Figure S3, the WF decreases from 4.3 to 4.0 eV for Al and from 4.8 to 4.25 eV for Au after the deposition of DNA. The decrease in WF of the contact metals assures a reduced electron injection barrier Φ_e.

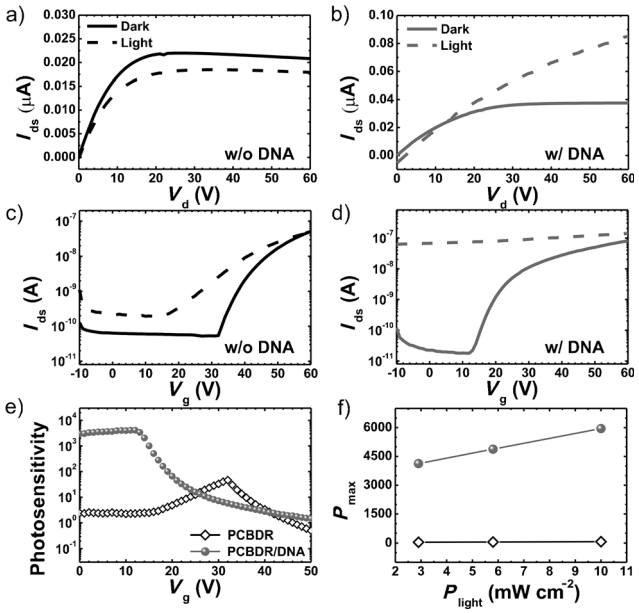

Figure 3. a) Output ($V_g = 60$ V) and c) transfer ($V_d = 60$ V) characteristics of the OPT ($W_{ch} = 1$ mm, $L_{ch} = 70$ μm) comprising of PCBDR without the DNA when measured in dark (solid lines) and under illumination (dashed lines, 2.9 mW cm^{-2}). b) and d) are according output and transfer curves for the PCBDR/DNA device. e) Photosensitivity of PCBDR and PCBDR/DNA devices versus the gate bias calculated based on dark and illuminated transfer curves. f) The maximal photosensitivity P_{max} as a function of irradiation intensity for PCBDR OPTs without and with the DNA layer.

Now we investigate the photoresponse of PCBDR OPTs with the presence of the DNA layer. Upon cw irradiation, the PCBDR device without DNA layers shows a decrease in I_{ds} for $1\ V \le V_d \le 60$ V. Similarly, we observe a decreased I_{ds} of the OPT with Au electrodes upon irradiation (see Figure S5a). In this regime of V_d, the device is operated in the on state and the I_{ds} is dominated by gate-induced carriers. Upon irradiation, extra charges (ρ_{photo}) are generated by photoexcitation and these charges are likely to recombine with the gate-induced carriers, leading to carrier losses in the OPT conduction channel. This process helps rationalize the decreased I_{ds} of PCBDR OPTs in this regime. In contrast, the I_{ds} of the OPT incorporating the DNA layer is enhanced upon irradiation, for example, from 0.037 to 0.085 μA for $V_d = +60$ V. Moreover we do not observe the saturation of I_{ds} upon irradiation for the PCBDR/DNA device. This is the signature of having excess charges in the active layer such that it is more difficult to pinch-off the channel conductivity. Figure 3c and 3d display transfer characteristics measured in dark and under irradiation of the two devices. For the PCBDR/DNA OPT, we observe a greater enhancement of I_{ds} for $V_g < V_{on}$. Consequently, the PCBDR/DNA OPT shows a much larger response of I_{ds} to light (see dashed line in Figure 4c and d). When operating the OPTs in the saturation regime with a higher V_g, we observe a further increase in I_{ds} for the PCBDR/DNA device. This indicates that the ρ_{photo} participates in the transport. The enlarged photoresponse can be rationalized by the increase in ρ_{photo} after irradiation. When operating the OPT in dark, with $V_g < V_{on}$, the carrier concentration and channel conductivity are both low. The current flowing between the drain–source electrodes is thus negligible, leading to an off state. We also compare the I_{ds} in dark of the two devices as shown in Figure S4b. The I_{ds} in the off state is not substantially raised after incorporating the DNA layer, which leads us to ruled out the possible mechanism of doping by DNA.[41] Thus the increase of I_{ds} in this regime is primarily attributable to the enlarged ρ_{photo} after irradiation. Based on transfer curves shown in Figure 3c and d, the photosensitivity (P) is calculated by Equation (1),[27,30]

$$P = \frac{I_{light} - I_{dark}}{I_{dark}} \quad (1)$$

where I_{dark} and I_{light} are the I_{ds} measured in dark and under illumination, respectively. Figure 3e compares the P of the

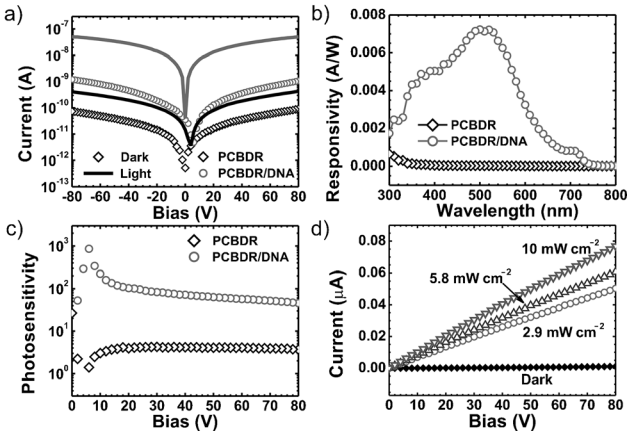

Figure 4. a) Current versus voltage (*I–V*) characteristics PCBDR and PCBDR/DNA lateral diodes ($W_{ch}=1$ mm, $L_{ch}=70$ μm) when measured in dark and under irradiation ($L_{power}=2.9\ mW\,cm^{-2}$). b) Steady-state photoconductivity of PCBDR and PCBDR/DNA films as a function of incident photon energy. c) Photosensitivity of the devices as a function of bias without and with the DNA layer. d) Linear scale *I–V* characteristics of the PCBDR/DNA lateral diode for measurements in dark and under various irradiation intensities.

two OPTs as a function V_g. After incorporating the DNA layer, the *P* of PCBDR transistors is enhanced by two orders with the maximal *P* (P_{max}) increased from 47 to 4118 when using Al electrodes. The V_g corresponding for the P_{max} also decreases from 32 V to 12 V due to the reduced V_{th}. In addition, we compared the P_{max} as a function of irradiation intensity. As shown in Figure 3 f, the gain in P_{max} when incorporating the DNA layer is more pronounced at higher irradiation intensity where charge recombination is more substantial due to the increase in the charge carrier density.[42] For the device with DNA, P_{max} increases linearly with increasing the P_{light}, further implying that carrier losses via the charge recombination may not be significant in the chosen range of P_{light}.

To further confirm the DNA-enhanced photoresponse, Figure 4 a shows current–voltage (*I–V*) characteristics of lateral diodes ($W_{ch}=1$ mm, $L_{ch}=70$ μm) comprising of PCBDR and PCBDR/DNA using Al top contacts. The dark current with the DNA layer is increased by one order, as a result of the reduced Φ_e. When irradiated at $2.9\ mW\,cm^{-2}$, the light current of the PCBDR/DNA device increases from 0.41 nA to 50 nA for $V=80$ V, leading to an over 100-fold enhancement in *P*. We also measured the photoresponse of the PCBDR lateral diodes to monochromatic photons. The photoresponsivity *R* (defined as $R=(I_{light}-I_{dark})/L_{power}$ with L_{power} for incident light power) of the two devices is shown in Figure 4 b as a function of incident photon energy. The *R* is greatly enhanced in the range of 300–700 nm with the DNA layer, for example, by 270 folds when irradiated by a monochromatic light of 500 nm. The *R* of the PCBDR/DNA device consistently matches the light absorption of the pristine PCBDR (see Figure S6) with the peak of *R* at about 500 nm. In stead, PCBDR control device shows a reduced and flat photoresponse in the visible region. Since both PCBDR and PCBDR/DNA display a similar absorption in solid state (see Figure S6 in the SI), the drastic changes of *R* confirm the enhancement of photoresponse by the DNA layer. Figure 4 c displays the *P* of PCBDR lateral diodes as a function of bias using Equation (1). On average, the *P* is 20 times higher after incorporating the DNA layer, giving a P_{max} of about 10^3. The *P* in Figure 4 b exhibits a weaker voltage dependence with the P_{max} that is slightly lower than that of the PCBDR/DNA OPT. This is mainly due to the lack of the gate dielectrics using lateral diode geometry so that the dark current cannot be entirely suppressed. Since the enhanced current of the lateral diode is purely due to the gain in the photoconductivity upon irradiation,[43] the channel conductivity R_{ch} should scale with the carrier concentration manipulated by the light intensity. Figure 4 c shows linear scale *I–V* characteristics of the PCBDR/DNA device in dark and under various irradiation intensities. The linearity of the *I–V* of the PCBDR/DNA device indicates an Ohmic current, resulting from the increase in ρ_{photo}. The slope of the *I–V* curves scales with the light intensity, producing a channel resistance (R_{ch}) of 7.4 GΩ in dark and a reduced R_{ch} from 1.6 GΩ to 1.0 GΩ for the light intensity increased from $2.9\ mW\,cm^{-2}$ to $10\ mW\,cm^{-2}$.

At last we explore the charge dissociation in PCBDR using transient absorption spectroscopy. Figure 5 shows the temporal evolution of the differential transmission ($\Delta T/T$) of

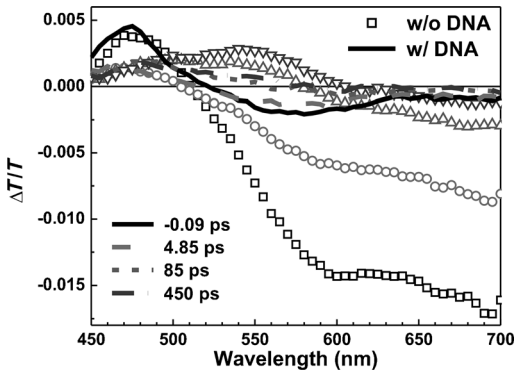

Figure 5. Temporal evolution of the transient absorption of PCBDR (symbols) and PCBDR/DNA (lines) films.

PCBDR and PCBDR/DNA films. Two features are visible for both: a ground-state bleach (GSB) peak initially occurring at 480 nm and a broad photoinduced absorption (PIA) in the range of 570–700 nm. The GSB peak is consistent to steady-state absorption of the PCBDR due to π–π* transition (see Figure S6 in the SI). At early times, the magnitude and shape of the GSB peaks of PCBDR and PCBDR/DNA are comparable. As contrary, the PIA band near 650–700 nm range for all the time probed here is significantly reduced for the PCBDR/DNA film in associated with a faster decay. Since the PIA originates from the absorption of the excited state excitons in PCBDR, the decrease in the PIA may indicate a higher dissociation rate of excitons in the presence of DNA. Note that the pump fluence used here (1 mJ per pulse) is unlikely to lead to a strong exciton–exciton annihilation which in turn can change the exciton decay kinetics. Because DNA has a HOMO and LUMO approximately of 7.6 eV and

2.8 eV, respectively as determined by ultraviolet photoemission spectroscopy (data not shown here), both the energy and charge transfers between the PCBDR and DNA should be restrained. In addition, because of the selected pumping energy, excitons are primarily created on the red-disperse dye moiety that possesses a smaller band gap than the fullerene moiety. Thus the energy transfer should be also suppressed between these two moieties in PCBDR. Based on these facts, the increased exciton dissociation indicated by the decreased PIA is likely to be due to interfacial effects possibly under the driving force of the dipole interaction at PCBDR/DNA interface. It is unclear about the detailed mechanisms of the photocurrent enhancement in the presence of the DNA layer.

To conclude, incorporation of thin DNA layers leads to a two-order enhancement of the photoresponse in PCBDR OPTs with a photosensitivity exceeding 10^3. The achievements are mainly attributable to improved exciton dissociation and electron injection manipulated by the DNA layer. The surface potential on PCBDR shows a higher response to irradiation when incorporating the DNA, which indicates that the density of surface charge carriers is enlarged upon irradiation by DNA. The enlarged photoresponse and surface carrier density are both rationalized by the dipole interaction at the PCBDR/DNA interface. Our results demonstrate a possibility of incorporating biomolecules into organic optoelectronics for light-detecting applications.

Experimental Section

The DNA was provided by the Air Force Research Laboratory from the Chitose Institute of Science and Technology and was kept in a desiccator before use. The PCBDR was synthesized as previously reported.[37]

DNA solutions were prepared by dissolving the DNA in H_2O:methanol (1:9 vol) solvent mixture. The DNA was first dissolved in ultra-pure water (18 MΩ) with a concentration of 10 mg mL^{-1}. After a sufficient stirring until the color turns clear, desired amount of anhydrous methanol was added into the DNA/water solution under N_2 environment, resulting in a total concentration of 1 mg mL^{-1}.

Si wafers with a 150 nm of thermally grown SiO_2 layer (Silicon Quest International) or glass substrates were sonicated in acetone and isopropanol sequentially. After drying, they were cleaned in a UV-O_3 oven before transferring in to a nitrogen purged glove box. The Si/SiO_2 surfaces were passivated by self-assembly of octyltrichlorosilane in hexane with a concentration of 0.1 vol%. The active layers were deposited from spin-coating solutions of PCBDR in chloroform with a concentration of 8 mg mL^{-1}, resulting in a film thickness of about 60 nm determined by a profilometer. Prior to the deposition of the DNA layer, the PCBDR films were pre-annealed at 150 °C for 15 min. The DNA solution was then spun-coat using a polyvinylidene (PVDF) filter atop the PCBDR at 2000 rpm for 60 s, producing an average DNA film thickness of 10 nm, as confirmed by AFM. The final step of device fabrication involves thermal evaporation of 80 nm Au drain–source electrodes through shadow masks, leading to a channel length of 70 μm and width of 1 or 2 mm. The samples were characterized in a Lakeshore vacuum probe station under vacuum (about 10^{-6} mbar) using a Keithley 4200 semiconductor parametric analyzer. Irradiation of the samples was implemented by shining cw white light from a xenon lamp (Spectra-Physics) filtered through an AM 1.5 G filter. The incident cw light was adjusted to be perpendicular to the active layer through a collimator. The light intensity was tuned by an optical filter wheel and calibrated by a NREL certified Si photodiode.

All AFM were measured in a N_2-purged glove box using the same films for the devices. Samples for EFM measurements were prepared by spin-coating the PCBDR atop pre-cleaned indium–tin oxide substrates. The DNA layers were prepared identically to the device fabrication. The topographic and EFM 1ω images were captured using a Multimode AFM (tapping mode) and Pt/Ir-coated silicon tips with a spring constant of about 5 N m^{-1} and resonant frequencies of 75 kHz. For the EFM measurements the lift height was remained 20 nm relative to the sample surface and the DC bias was applied externally by a Keithley 2000 multimeter onto the ITO substrates.

XPS and UPS were measured by a Kratos Ultra spectrometer in a vacuum of 1×10^{-9} Torr using monochromatized $Al_{K\alpha}$ X-ray photons for the XPS ($h\nu = 1486.6$ eV) and a HeI discharge lamp for the UPS ($h\nu = 21.2$ eV). PCBDR and PCBDR/DNA films were spin-coated on SiO_2 substrates that were pre-evaporated with 50 nm of a Au layer. The pass energy and step size were 80 and 0.5 eV for the XPS and 5 and 0.025 eV for the UPS. The XPS data were analyzed by the CASA XPS software (Version 2.3).

The WFs of Al and Au with and without deposition the DNA layer were measured by a frequency-modulated scanning Kelvin probe microscopy (SKPM) using a platinum-coated tip with a resonance frequency of 275 kHz in N_2 atmosphere. SKPM experiments were done in custom code based on that provided by the Ginger laboratory for Igor Pro and the Asylum Research XOP as described elsewhere.[44]

The surface contact potential difference (CPD) measurements were carried out by using a KP technology integrated Kelvin probe system and a stainless tip with applying an AC bias of ±7 V and oscillation frequency of 70 Hz. The determined CPD is relative to a Au reference which has a calibrated WF of 5.1 eV. The irradiation was provided by a Dolan–Jenner fiber optic system coupled with a halogen light source and the light intensity was controlled by a glovebox Scanning Kelvin Probe & Surface Photovoltage System program and calibrated by a power meter.

Steady-state photoconductivity was performed on PCDBR (or PCBDR/DNA) by using a monochromatic light sourced by a tungsten lamp. The films were prepared on pre-cleaned alumina substrates by spin-coating. Lateral device geometry was used constituting two thermally evaporated gold electrodes with a gap of 50 μm. The incident light beam was mechanically chopped at 170 Hz before shining on the samples and an electric field of 6.0×10^4 V cm^{-1} was applied to collect the current. The samples were measured in dynamic vacuum ($< 10^{-4}$ mbar). The spectral dependence of the incident light beam was pre-calibrated using a calibrated Si photodiode.

Transient absorption spectra were collected by using a Spectra-Physics Millennia Vs 532 nm continuous wave laser pumping a Spectra-Physics Tsunami Ti:Sapphire laser (150 fs pulse at 800 nm, repetition rate of 1 kHz), amplified by a Spectra-Physics Spitfire amplifier, which generated a 1 mJ pulse with a width of 140 fs and a repetition rate of 1 kHz. The pump was sent through an optical parametric amplifier (OPA), allowing for a wavelength tuning from 600–750 nm. The pump was delayed with a chopper and focused with a spot size of about 800 μm onto a sample. The differential transmission ($\Delta T/T$) signal was collected by a monochromator and detector with scanning the wavelengths of the collected probe and varying the delay of the pump.

Received: August 1, 2013
Published online: November 18, 2013

Keywords: DNA · exciton dissociation · interfacial dipole · photoresponsive materials · thin films

[1] C. D. Dimitrakopoulos, P. R. L. Malenfant, *Adv. Mater.* **2002**, *14*, 99.
[2] S. R. Forrest, *Nature* **2004**, *428*, 911.

[3] G. Horowitz, *Adv. Mater.* **1998**, *10*, 365.
[4] J. E. Anthony, *Chem. Rev.* **2006**, *106*, 5028.
[5] A. L. Briseno, S. C. B. Mannsfeld, M. M. Ling, S. H. Liu, R. J. Tseng, C. Reese, M. E. Roberts, Y. Yang, F. Wudl, Z. N. Bao, *Nature* **2006**, *444*, 913.
[6] C. L. Wang, H. L. Dong, W. P. Hu, Y. Q. Liu, D. B. Zhu, *Chem. Rev.* **2012**, *112*, 2208.
[7] D. S. Weiss, M. Abkowitz, *Chem. Rev.* **2010**, *110-110*, 479.
[8] V. Podzorov, V. M. Pudalov, M. E. Gershenson, *Appl. Phys. Lett.* **2004**, *85*, 6039.
[9] D. Amarasinghe, A. Ruseckas, G. A. Turnbull, I. D. W. Samuel, *Proc. IEEE* **2009**, *97*, 1637.
[10] X. Gong, M. H. Tong, Y. J. Xia, W. Z. Cai, J. S. Moon, Y. Cao, G. Yu, C. L. Shieh, B. Nilsson, A. J. Heeger, *Science* **2009**, *325*, 1665.
[11] J. J. Wang, Y. Q. Wang, F. F. Cao, Y. G. Guo, L. J. Wan, *J. Am. Chem. Soc.* **2010**, *132*, 12218.
[12] N. Marjanovića, Th. B. Singha, G. Dennlera, S. Günesa, H. Neugebauera, N. S. Sariciftcia, R. Schwödiauerb, S. Bauerb, *Org. Electron.* **2006**, *7*, 188.
[13] C. H. Kim, M. H. Choi, S. H. Lee, J. Jang, S. Kirchmeyer, *Appl. Phys. Lett.* **2010**, *96*, 123301.
[14] S. W. Jeong, J. W. Jeong, S. Chang, T. Y. Oh, S. Y. Kang, K. I. Cho, B.-K. Ju, *Sens. Actuators B* **2011**, *156*, 657.
[15] X. Wang, K. Wasapinyokul, W. D. Tan, R. Rawcliffe, A. J. Campbell, D. D. C. Bradley, *J. Appl. Phys.* **2010**, *107*, 024509.
[16] S. Jeon, S.-E. Ahn, I. Song, C. J. Kim, U.-I. Chung, E. Lee, I. Yoo, A. Nathan, S. Lee, J. Robertson, K. Kim, *Nat. Mater.* **2012**, *11*, 301.
[17] G. Hernandez-Sosa, N. E. Coates, S. Valouch, D. Moses, *Adv. Funct. Mater.* **2011**, *21*, 927.
[18] G. Yu, J. Gao, J. C. Hummelen, F. Wudl, A. J. Heeger, *Science* **1995**, *270*, 5243.
[19] P. Peumans, A. Yakimov, S. R. Forrest, *J. Appl. Phys.* **2003**, *93*, 3693.
[20] J. W. Levell, M. E. Giardini, I. D. W. Samuel, *Opt. Express* **2010**, *18*, 3219.
[21] J. Zaumseil, H. Sirringhaus, *Chem. Rev.* **2007**, *107*, 1296.
[22] E. C. P. Smits, T. D. Anthopoulos, S. Setayesh, E. van Veenendaal, R. Coehoorn, P. W. M. Blom, B. de Boer, D. M. de Leeuw, *Phys. Rev. B* **2006**, *73*, 205316.
[23] K. S. Narayan, N. Kumar, *Appl. Phys. Lett.* **2001**, *79*, 1891.
[24] T. P. I. Saragi, R. Pudzich, T. Fuhrmann, J. Salbeck, *Appl. Phys. Lett.* **2004**, *84*, 2334.
[25] M. C. Hamilton, S. Martin, J. Kanicki, *IEEE Trans. Electron Devices* **2004**, *51*, 877.
[26] Y. Xu, P. R. Berger, J. N. Wilson, U. H. F. Bunz, *Appl. Phys. Lett.* **2004**, *85*, 4219.
[27] Y. Guo, G. Yu, Y. Liu, *Adv. Mater.* **2010**, *22*, 4427.
[28] T. P. I. Saragi, T. Spehr, A. Siebert, T. F. Lieker, J. Salbeck, *Chem. Rev.* **2007**, *107*, 1011.
[29] M. Y. Cho, S. J. Kim, Y. D. Han, D. H. Park, K. H. Kim, D. H. Choi, J. Joo, *Adv. Funct. Mater.* **2008**, *18*, 2905.
[30] M. E. Gemayel, M. Treier, C. Musumeci, C. Li, K. Müllen, P. Samorì, *J. Am. Chem. Soc.* **2012**, *134*, 2429.
[31] A. L. Briseno, S. C. B. Mannsfeld, C. Reese, J. M. Hancock, Y. Xiong, S. A. Jenekhe, Z. Bao, Y. Xia, *Nano Lett.* **2007**, *7*, 2747.
[32] C. W. Struijk, A. B. Sieval, J. E. J. Dakhorst, M. Van Dijk, P. Kimkes, R. B. M. Koehorst, H. Donker, T. J. Schaafsma, S. J. Picken, A. M. Van de Craats, J. M. Warman, H. Zuilhof, E. J. R. Sudholter, *J. Am. Chem. Soc.* **2000**, *122*, 11057.
[33] P. Zalar, D. Kamkar, R. Naik, F. Ouchen, J. G. Grote, G. C. Bazan, T.-Q. Nguyen, *J. Am. Chem. Soc.* **2011**, *133*, 11010.
[34] Y. Zhang, P. Zalar, C. Kim, S. Collins, G. C. Bazan, T.-Q. Nguyen, *Adv. Mater.* **2012**, *24*, 4255.
[35] X. Y. Cheng, Y. Y. Noh, J. P. Wang, M. Telle, J. Frisch, R. P. Blum, A. Vollmer, J. P. Rabe, N. Koch, H. Sirringhaus, *Adv. Funct. Mater.* **2009**, *19*, 2407.
[36] B. de Boer, A. Hadipour, M. M. Mandoc, T. van Woudenbergh, P. W. M. Blom, *Adv. Mater.* **2005**, *17*, 621.
[37] M. Wang, E. Chesnut, Y. Sun, M. Tong, M. Guide, Y. Zhang, N. D. Treat, A. Varotto, A. Mayer, M. L. Chabinyc, T.-Q. Nguyen, F. Wudl, *J. Phys. Chem. C* **2012**, *116*, 1313.
[38] O. Cherniavskaya, L. Chen, M. A. Islam, L. E. Brus, *Nano Lett.* **2003**, *3*, 497.
[39] L. Chen, O. Cherniavskaya, A. Shalek, L. E. Brus, *Nano Lett.* **2005**, *5*, 2241.
[40] O. Cherniavskaya, L. Chen, V. Weng, L. Yuditsky, L. E. Brus, *J. Phys. Chem. B* **2003**, *107*, 1525.
[41] F. Maddalena, E. J. Meijer, K. Asadi, D. M. de Leeuw, P. W. M. Blom, *Appl. Phys. Lett.* **2010**, *97*, 043302.
[42] Y. Zhang, X.-D. Dang, C. Kim, T.-Q. Nguyen, *Adv. Energy Mater.* **2011**, *1*, 610.
[43] D. Gupta, T. J. K. Brenner, S. A. Seifried, M. J. Lee, M. Heeney, I. McCulloch, H. Sirringhaus, *Org. Electron.* **2012**, *13*, 36.
[44] L. S. C. Pingree, D. B. Rodovsky, D. C. Coffey, G. P. Bartholomew, D. S. Ginger, *J. Am. Chem. Soc.* **2007**, *129*, 15903.

